Morphological analysis of as-manufactured filament wound composite cylinders using contact and non-contact inspection methods

Morphological Analysis of As-Manufactured Filament Wound Composite Cylinders Using Contact and Non-Contact Inspection Methods

Emanuela Natale[1], Antonella Gaspari[2], Luciano Chiominto[1*], Giulio D'Emilia[1], Antonios G. Stamopoulos[1]

[1]Department of Industrial and Information Engineering and Economy (DIIIE), University of L'Aquila, Via Giovanni Gronchi, 18, Nucleo Industriale Pile L'Aquila, 67100, Italy

[2]Department of Mechanics Mathematics and Management (DMM), Polytechnic of Bari, Via Orabona, 4, Bari, 70125, Italy

Highlights

- **Assessment of the applicability of contact and non-contact methods for detecting morphological and structural defects.**
- **Analysis of the thickness variation of as-manufactured filament winded cylindrical structures.**
- **Identification of discontinuities through-the-thickness implementing portable ultrasound inspection system.**
- **Measurement of the winding angle with optical/vision system.**
- **Identification of the repeatability of the process outcome.**

Abstract

Filament winding is a versatile technique for producing pressure vessels throughout the deposition of continuous fiber filaments on a rotating mandrel under determined conditions. Due to its simplicity as a fabrication process, it has been gaining significant interest by the pressure vessels industry in general. Considering the relative safety requirements, these structures are expected to demonstrate high load carrying capacity to ensure the proper storage and transportation of pressurized fuels. To this end, fiber reinforced polymers have been employed for meeting the structural requirements that are often susceptible to many defects. Therefore, the quality of the manufactured product and the identification of these defects, both structural and morphological, is essential. In the present work, measurements have been conducted in as-manufactured filament wound cylinders made of carbon fiber reinforced polymer for identifying their morphological characteristics and the presence of variations of the winding angle and gaps or voids. Both contact and non-contact techniques were applied, and their applicability was further assessed. The results revealed deviations between the designed and manufactured product, giving insights that are

* Corresponding Author: Luciano Chiominto, email: luciano.chiominto@graduate.univaq.it

useful for understanding the fabrication process and its outcome and for further implementation of the abovementioned techniques in a quality assessment protocol.

Keywords: Composites, Manufacturing Defects, Filament Winding, Defects, Ultrasound Inspection, Vision system

1.Introduction

The filament wound composites are used in many industrial sectors, especially when the products are axial symmetric components such as tubes or pressure vessels [1-2]. As a manufacturing process, dry filament winding copes with the deposition of continuous fibers onto a continuously rotating mandrel. Throughout the recent years, there have been observed some variations of the same process, including the implementation of both thermoplastic and thermoset based polymeric systems, such as the wet or resin-bath winding [3], dry or tape winding [3-5], laser assisted [4] or even using electrostatic spray assisted methods [6]. In the case of wet winding, the fibers are obliged to pass through a resin bath before their deposition to the mandrel [3]. This method requires specific resin systems that are kept in special conditions in the resin bath to avoid the preliminary degradation and to enhance the proper penetration of the resin inside the fiber filaments. The obvious alternative solution, the dry winding, deals with the utilization of pre-impregnated fibers, in the case of thermoset-based tows, that are simply stored in specific conditions before their implementation in the fabrication process. Within this method, the tow dimensions are more easily controlled since a dedicated machine produces the tows independently and in a more efficient manner [7]. In general, the filament winding process is considered among the most cost effective and highly automated manufacturing processes for producing axial-symmetrical composite products.

Since the filament winding process method is utilized for producing pressure vessels or tubes that are subjected to high internal pressure, the products have to meet high levels of structural performance for safety reasons. Therefore, the accurate detection and minimization of the defects caused by the fabrication process is essential. These defects may be divided into 2 major categories, namely those related to the tows and the related impregnation, such as unstable tow width or intrafilamentary porosity, and those related to the filament winding process. For instance, large voids may be introduced by the process as seen in the work of Scott et al. [8] where the void content in filament wound structures was studied by means of high-resolution computed tomography. It was presented a large number of large voids that correspond to gaps between consecutive deposited tows of the same layer. Another critical issue is the fiber waviness, in or out of plane, that results a local deviation from the stable designed fiber orientation. In the work of Faria [9] the fiber waviness and misalignment were identified as a process induced phenomenon that was developed in and out of plane locally. In the same context, Stecenko and Piggott [10-11] presented fiber deviation and waviness as a phenomenon that is frequently present in

filament wound tubes. The effect of such kind of phenomena may degrade the whole structure locally, introducing a form of damage that was introduced by the fabrication process. In this context, both the fiber orientation and the wall thickness of filament wound composite structures may affect the quasi static and dynamic compressive behaviour significantly, as shown in the work of Wang et al. [12].

Considering the above, since the introduction of these defects may cause preliminary failures to the whole structure, their accurate evaluation can be exploited both for the component analysis but also for the process quality assessment and be the base for further improvements of the fabrication process. In this framework there has been reported a wide range of techniques for detecting and measuring the extent of these defects. In the work of Johnson and Nokes [13] the effectiveness of several non-destructive techniques such as acoustic emission, ultrasound, shearography and radiography was assessed. Acoustic emission was implemented in similar filament wound structures by Downs and Hamstad [14]. In addition, Lee et al. [15] examined the impact damage in filament wound pressure vessels using a system based on laser ultrasonic transmission. Finally, the porosity, from micro to macro level in glass/epoxy filament wound pressure vessels was studied by Srivastava et al. [16] using micro computed tomography. Since every non-destructive technique demonstrates several limitations, among the most promising techniques for fast and efficient identification of such kind of defects in composite structures are the ultrasound inspection [17-19] and the optical/vision systems [20-21].

In the present work, the applicability of two of the most frequently used inspection methods when applied to as-manufactured composite filament wound cylinders is evaluated. These structures are representative of the cylindrical part of a pressure vessel, fabricated using commercial products (fibers, epoxy resin) for fabricating the tows. A contact-based ultrasound system is utilized for measuring the wall thickness and for assessing the presence of gaps between the various layers. In addition, a vision system is utilized for scanning and measuring the variability of the winding angle. Assessment of the measurement uncertainty of experimental data of both measuring methods is a key factor to use this information for improvement of the fabrication process.

From the results, the potential of each method is presented and valuable information about the consistency of the fabrication is examined. The hollow cylinders appear to have variations in the winding angle and an accumulation at both ends of the structure.

2.Material and Methods

2.1 Materials and Fabrication

The composite cylinders manufactured herein are made of carbon/epoxy towpregs, where the carbon fibre is the Toray T700S-12K-50C and the whereas the epoxy resin system is the Huntsman Araldite Solution composed of the Araldite LY 3508 epoxy resin, the Aradur 1571 hardener and the Accelerator 1573 accelerator. The fiber impregnation for creating the towpregs was conducted by the COMEC

Innovative srl (Chieti, Italy) using the multistep TowPreg machine at roughly 70ºC. The nominal width of the produced tows was approximately 7 mm. The filament winding non-geodesic procedure was conducted using a commercial full-scale 3-axis winder (COMEC Innovative srl, Chieti, Italy). A collapsible cylindrical mandrel made of stainless steel with a diameter of 200 mm and 300 mm length was considered with removable tapered ends, as shown in Fig.1. The winding angle was approximately 60º. Nevertheless, for ensuring the proper deposition of the tows, 1 hoop layer (90º) was first deposited and roughly 44 layers of helicoidally wound layers were deposited onto the hoop ones). After the winding process, the composite structure was cured attached to the mandrel in 120 ºC for 2 h and 140 ºC for 2h respectively using an oven without vacuum. A critical aspect is the extraction of the cylinder from the mandrel. For this reason, a polyimide film was meticulously applied onto the mandrel, as seen in Fig.1 as well.

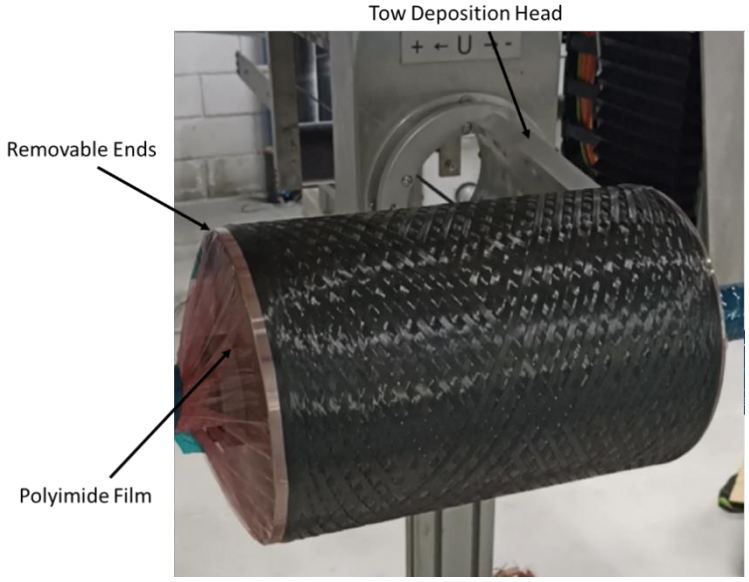

Fig. 1: Instant from the filament winding process and the configuration of the machine/mandrel.

2.2 Measuring Methods

As previously stated, the measuring methods in this work are both contact and non-contact. For the contact method, a pulse-echo ultrasound measurement technique was selected since it is considered among the most promising techniques for this kind of inspection [22]. Considering the non-contact methods, a vision system is used to analyze the morphology of the tows in terms of winding angle. Regarding the ultrasound system, an uncertainty evaluation has been conducted prior to the cylinders inspection.

2.2.1 Ultrasound inspection system

The ultrasound inspection is implemented for assessing the presence of large discontinuities through-the-thickness and for obtaining the wall thickness variation. To this end, the contact pulse-echo technique is put into practice. The ultrasound equipment is a portable Waygate USM 100 transmitter-

receiver system with a 2.25 MHz contact probe, presented in Fig.2 (a). The selected probe has a diameter of the transducer element of 7.6 mm and is also equipped with a 9 mm acrylic delay line to improve the near surface resolution. An ultrasonic gel couplant is used between the probe and the component for permitting the transmission of ultrasonic energy from the transducer into the specimen. Regarding the instrument parameters, the pulser is set to a voltage of 200 V and a width of 222 ns. For the receiver, the filter is set to 2.25 MHz and the damping resistance is 50 Ω. Consequently, a calibration to evaluate the ultrasound velocity was conducted on the cylinder to a point where the entire thickness of the component is easily detectable. During the calibration phase, the reference thickness is 5.50 $\pm$ 0.01 mm, and the evaluated speed of sound is 2947 $\pm$ 12 m/s.

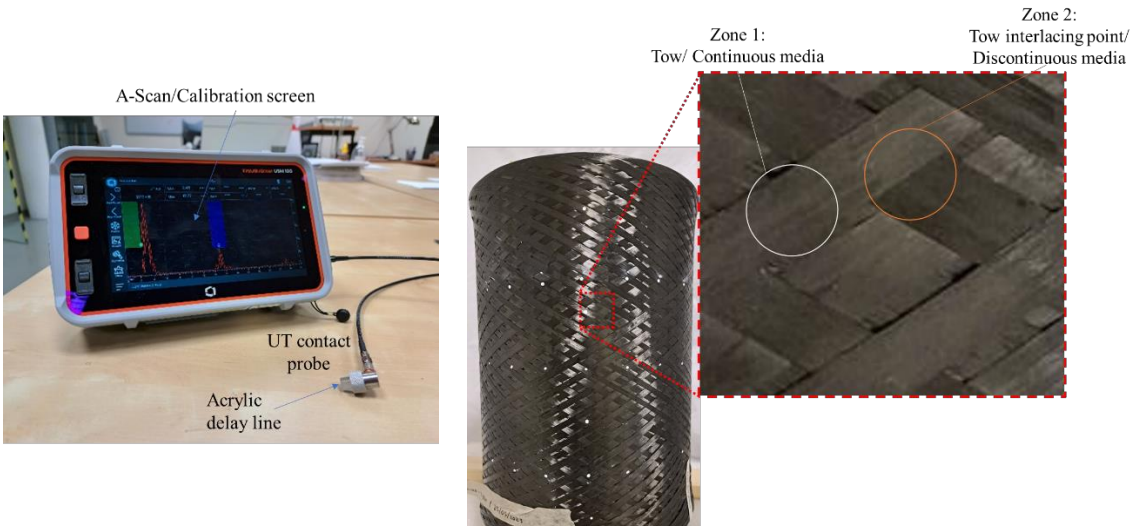

Fig. 2: The Waygate USM 100 ultrasound inspection system utilized in the present work(a) and the details of the scanned zones of the interlaced tows (b).

The uncertainty of the measuring system, that is the result of the synergy of different phenomena/parameters related to the material, the morphology of the geometry, and the settings of the instrument, is not provided by the system manufacturer. During the calibration phase, the accurate determination of the time-of-flight that corresponds to the time for a certain wavelength to cross the entire thickness is required. Another important factor is the surface roughness that influences ultrasound dissipation [23]. Each of these factors was studied to assess the uncertainty of the thickness measurement. The speed of sound estimation uncertainty was estimated considering blocks of known dimension of the same material. For the system setting, the most influential ones are the filter and the damping resistance. To evaluate the uncertainty linked to these factors a design of experiment was defined. For the filter option three different frequencies were selected: 1.00 MHz, 2.25 MHz, and 4.00

MHz. For the damping resistance, the only available options were 50 Ω and 400 Ω. Also considering the complexity of the filament wound structure, the interlaced tows are introducing a complex surface that is composed of rhomboidal units that are repeated. This outer surface may introduce further difficulties on the applicability of the contact ultrasound system. Therefore, measurements were carried out on 2 different zones, namely on the distinct tow surface and on the gap between interlaced tows as seen in Fig.2(b). The interlaced zone was found to increase the noise of the measurement and altered the obtained A scan. Therefore, to eliminate any interference of the morphology of the interlaced tows, Zone 1 was selected for further assessment of the characteristics of the filament wound structure.

2.2.2 Vision system and uncertainty assessment

As previously stated, in an ideal helical winding pattern, the tows are wound at an angle α to longitudinal axis of the cylinder/mandrel, as seen in Fig.3. Therefore, in a rhomboidal pattern that is created, the winding angle α is the difference between 90^o and the angle β.

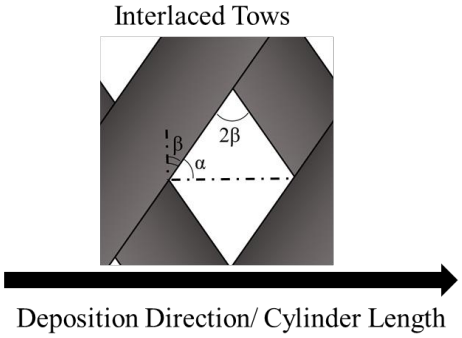

Fig. 3: Scheme of the angles in a helicoidal winding pattern

For measuring the winding angle, a vision system, presented in Fig. 4 (a), composed of a Dalsa Genie Nano C4040 color camera with a resolution of 4112x3008 pixels is utilized. This particular configuration has been proven to be efficient for measuring the variation of the angles between the fiber strands in woven fabrics as seen in past works [24]. The lighting system is composed of two soft boxes with 80 W bulbs. During the calibration phase, the components are placed 190 mm away from the camera. The images are acquired using an aperture of f/8 with an exposure time of 150000 μs.

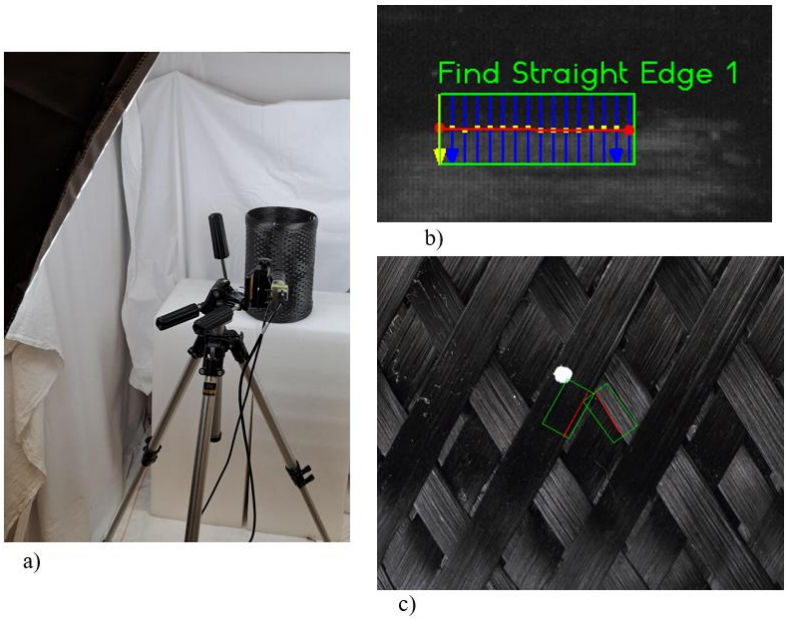

Fig. 4: Vision system used to analyze the surface of the cylinder (a). ROI for edge identification. The search lines are in blue, and the identified edge is in red (b). Identified edges of a pair of adjacent elements of the weave

Vision Builder for Automated Inspection is used to analyze the images of the surface. In particular, the Find Straight Edge function is used to identify the edge of a tow. This function defines a region of interest (ROI) as seen in Fig. 4 (b). Consecutively, the intensity difference of the pixels along a specific number of lines within a defined path is calculated. The maximum difference of this quantity identifies a point of discontinuity that corresponds to an edge. Finally, a fitting of the identified points provides the searched edge. The straight edge of the single tow is represented by a vector. Therefore, the tow angle is defined by the difference between the vectors that represent the edges of a pair of adjacent elements of the interlaced tows, as seen in Fig 4 (c).

The image processing method was validated using a reference image with all angles of 90°. This test produced satisfactory results with the angle value centered on 90° and a variability of repeated measures in the order of hundredths of a degree. The main contributions to the uncertainty of the measuring system were identified and evaluated. To reduce distortions due to the shape of the component and the optical system, the object was placed in the middle of the acquired area. The repeatability of the method was assessed by conducting three repeated measurements on the same couple of tows on three different images. Then, the maximum difference of the angles was calculated. The resolution of the image is determined by the resolution of the camera and the working distance. Their effects were evaluated considering the maximum angle variation due to the resolution. The maximum variation of the measured angle due to the main parameters of the processing algorithm was assessed with a sensitivity analysis. The influence of lighting system is estimated by changing the number of illuminators, one or two, and their distance from the component, 500 – 1500 mm. In all cases, the uncertainty contributions were determined using a rectangular probability distribution.

3. Experimental

The 2 filament wound cylinders studied in the present work are reported in Fig.5. For excluding the influence of several fabrication parameters and for assessing the repeatability of the manufacturing method, they are both wound by the same carbon/epoxy system, same material quantity, nominal winding angle and deposition parameters. They both consist of 1 layer of hoop wound prepreg tows while the rest is helicoidally wound, as described in section 2 of the present work.

(a) (b)

Fig. 5: The cylinder A (a) and B (b) studied in the present work.

Both components are inspected using the ultrasound system and the vision system to study their thickness trend and the winding angle variation. For performing the thickness measurements, the 2 cylinders were divided into distinct zones, 2 lines (LL) parallel to the longitudinal axis and 3 circumferences, as seen in Fig.6 (a). Therefore, also considering the notable dimensions of the tubes, a grid was introduced through which the necessary measurements are conducted locally. The 2 longitudinal lines, namely LL1 and LL2, are considered at approximately 70° distance between them and are composed of 29 points, presented in Fig.6 (b) with the white spots, that cover the whole length of the tube, each of them 10 mm distant from the subsequent one.

(a)

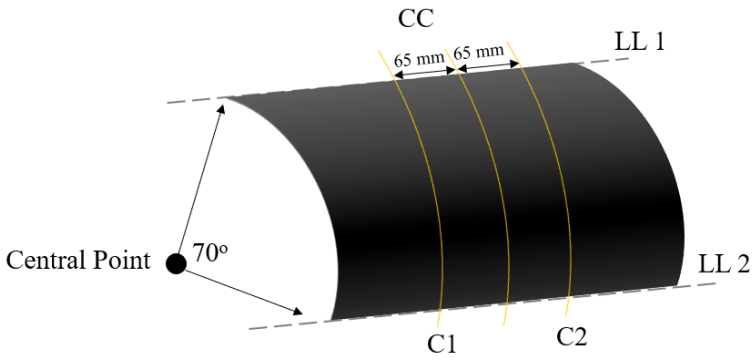

(b)

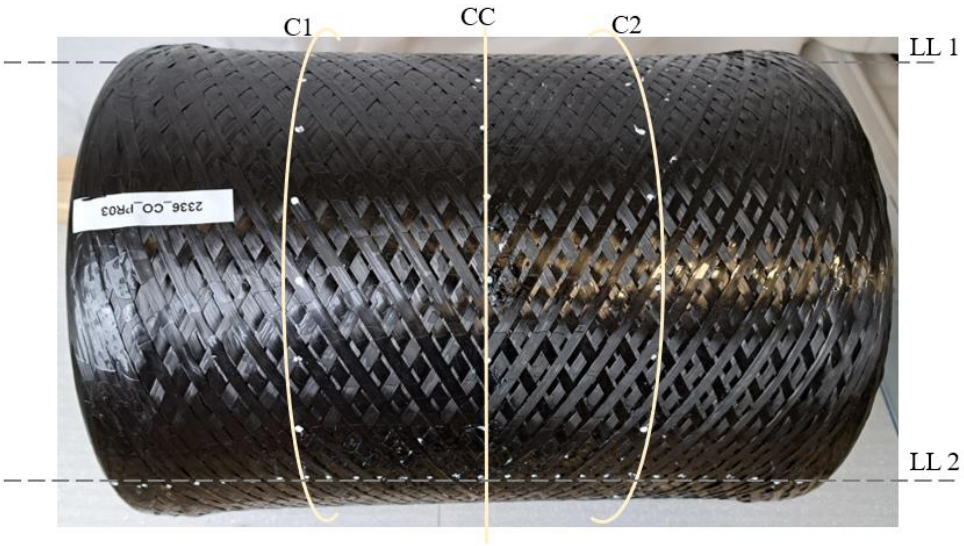

Fig. 6: The subdivision of the component into distinct zones of measurements

For the circumferential measurements 3 slices were considered, namely the central circumference (CC), the top (C1) and bottom one (C2), as seen in Fig.6. The CC corresponds to the most central circumference of the cylinder since it is considered at half of the length of the cylinder. The C1 and C2 are placed 65 mm left and right respectively, as seen in Fig.6 (a). Each of the circumferences is composed of 22 points every 16º approximately, as seen in Fig.6 (b). As explained in Section 2.2.1 of the present work, the measurements were conducted in zones on the top of an external tow, avoiding discontinuities of the material that could potentially affect the quality of the ultrasound. For calibration purposes, the point where the front and backwall of the ultrasound are detected without any severe defects was considered as reference. In the present case, the nominal thickness value was 5.5 mm. The measurement was provided by a high-precision micrometer.

4. Results and Discussion

4.1 Uncertainty Assessment of the Ultrasound and Vision-Based Systems Measurements

The uncertainty of the thickness measurement and the winding angle is evaluated. For each measurement the assessment procedure is described in Section 2. Herein, the percentage uncertainty of the thickness measurement has been evaluated as the sum of the square roots of the parameters listed in Table 1, that is the variability of the speed of the ultrasound and the related repeatability, the repeatability of the measurement overall, the precision of the system settings applied to the present case and the overall repeatability of the measurements. Each of the parameters contributes to the overall uncertainty differently while the ultrasound system settings appear to be the prominent parameter. For the helicoidally wound composite components with a nominal thickness in the order of 5.5 mm the overall uncertainty is roughly 0.06 mm, that corresponds to 1%.

Table 1: Uncertainty contributions to the ultrasound thickness measurement

Parameter	Percentage Variability [%]	Uncertainty contribution [mm]
Sound speed estimation	0.4	0.02
Repeatability of sound speed	0.1	0.01
Reference value	0.2	0.01
System settings	0.6	0.03
Repeatability	0.2	0.01

For the winding angle measurements, the parameters that may cause an uncertainty are listed in Table 2. In this case, the accuracy of the optical inspection with a vision-based system may be affected by the set-up, the resolution of the equipment and the image obtained as well as by the illumination conditions. With reference winding angle of 60^o, the percentage variability is in the order of 1.1% or 0.66^o. These values are considered satisfactory for the morphological analysis of the cylindrical structures. Considering the abovementioned accuracy of both systems and despite the cylindrical shape and the tow wound composite structure, both systems are assumed to provide satisfactory values for the analysis of the thickness and the winding angle variation.

Table 2: Uncertainty contributions to the winding angle measurement

Parameter	Percentage Variability [%]	Uncertainty contribution [Degree]
Repeatability	0.5	0.3
Resolution	0.5	0.3
Parameter set-up	0.7	0.4
Lighting	0.5	0.3

4.2 Morphology of the Winded Cylinders

4.2.1 Wall Thickness

The 2 typical cases of the signal received are presented in Fig.7 for the case of a filament wound structure with and without defect, stating a typical pulse-echo analysis. The first peak of the A-scan corresponds to the external surface while, in the case of the presence of a defect such as a delamination or a gap, there can be observed 3 peaks where the 2^{nd} one corresponds to the discontinuity.

(a) Pulse-Echo with no defect

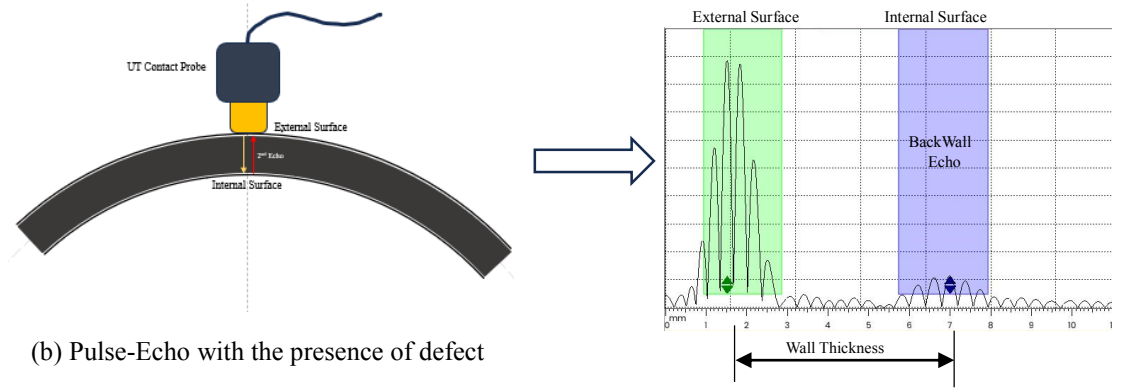

(b) Pulse-Echo with the presence of defect

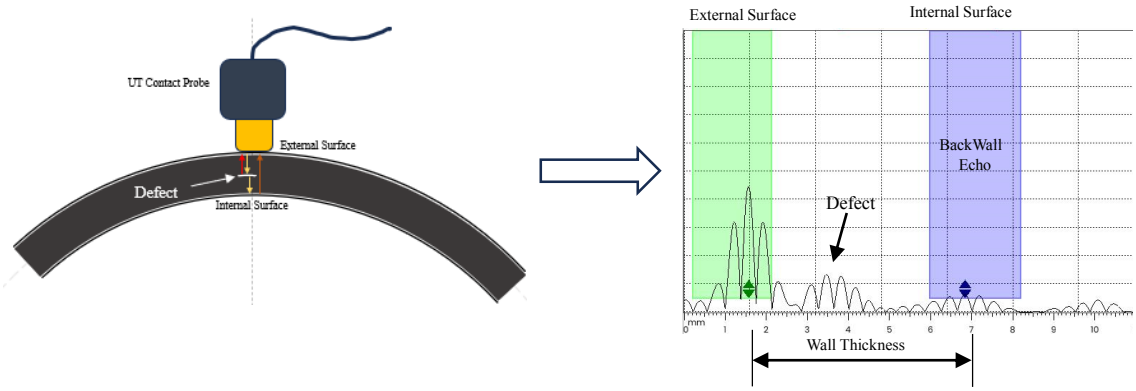

Fig. 7: Schematic description and the corresponding A-scan for the case of a cylindrical, filament wound, composite structure without (a) and with a discontinuity (b).

As seen in Fig.7, the time of flight (ToF), that is the time required for the ultrasound to travel throughout the composite structure, is utilized for the calculation of the thickness. The thickness values may be obtained by the distance between the first peak and the backwall echo. Also considering the complexity of the filament wound structure, multiple defects in more than 1 level through the thickness may be present. This fact may affect the calculation of the overall wall thickness of the composite cylinder due to the presence of multiple peaks that make almost the back wall echo almost undetectable. In this case, the value of the backwall echo was taken by linear extrapolation using the values of the previous and the next point of measurement. The distribution of the wall thickness across the 2 longitudinal lines of the 2 cylinders are presented in Fig.8. As seen in all the cases, there is an oscillation of the first echo caused by the roughness of the external surface of the interlaced tows. On the other hand, the backwall echo appears to be stable mostly between the 5th and 22nd points of the measuring lines that correspond to the central part of the cylinder, also considering the presence of hoop wound tows that are highly compacted to the mandrel compared to the external helical ones.

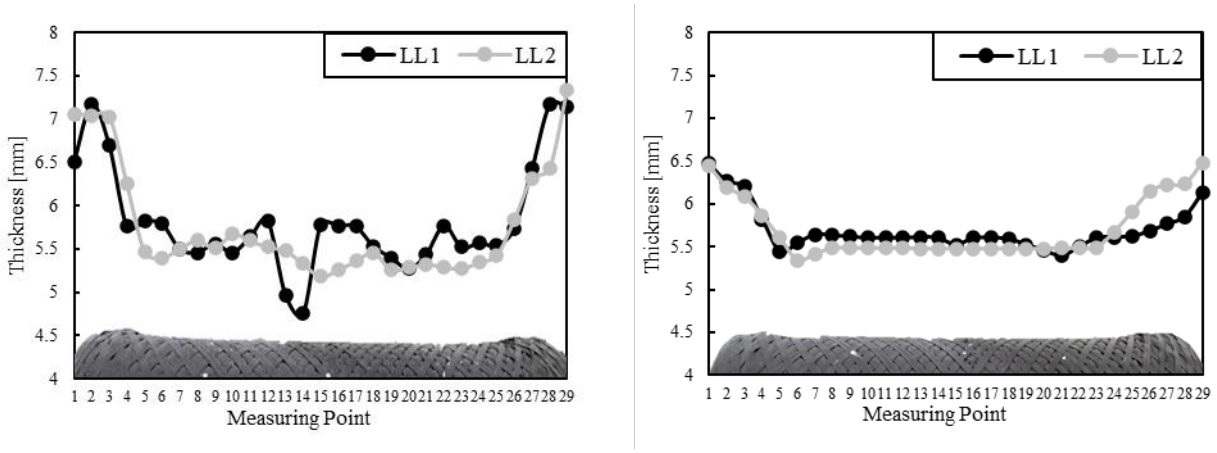

Fig. 8: Variation of the echoes and the wall thickness along the measuring points of the 2 longitudinal lines for the 2 filament wound cylinders: (a) Cylinder A; (b) Cylinder B.

In fact, the increased thickness of the 2 ends of the filament wound structure is evident even by an optical observation and is caused by a series of fabrication characteristics such as the accumulation of material in the case of delay of the tow deposition head, the reduced compaction and, partially, the folding of the tows due to the movement of the mandrel and the head as well.

The wall thickness measured in the 3 circumferences C1, CC and C2 is presented in Fig.10 for the Cylinder A (Fig.9(a)) and B (Fig.9(b)) respectively. The distribution of the thickness is found to be irregular, achieving values between 4.7 and 7.5 mm for the Cylinder A and between 5.3 and 6.5 mm for the case of the Cylinder B. In general, the central circumference appears to be more compacted, presumably due to the higher tension applied to the tows during the winding process that leads to higher compaction and, consequently, to a denser filament wound composite structure [25-26].

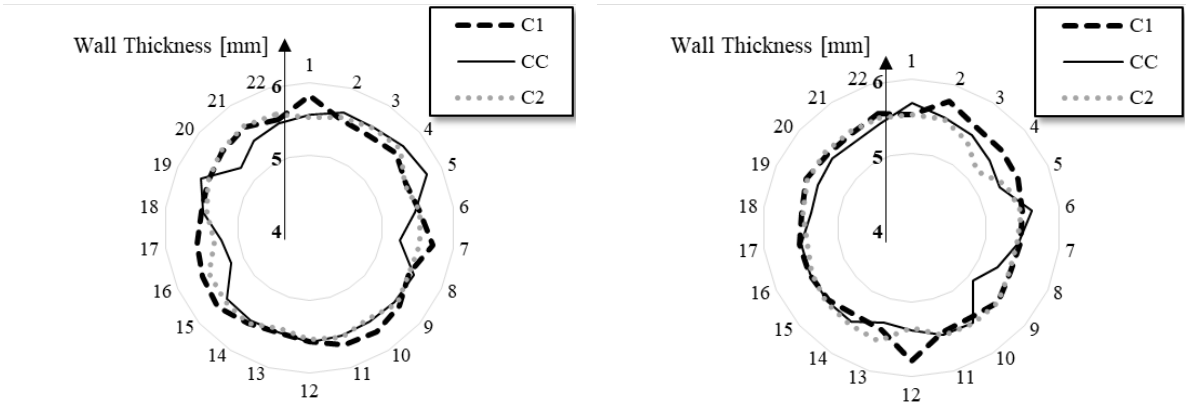

Fig. 9: The wall thickness distribution as measured in the points of the 3 circumferences of the Cylinder A (a) and B (b) respectively.

The mean values of the thickness of the 2 cylinders are presented in Fig.10 for all the measured point lines. The average wall thickness for the 2 hollow cylinders was found to be 5.65 and 5.76 mm respectively. Even though the 3 circumferences are located in the central cylindrical part, there can be observed a slightly more compacted central circumference (CC) compared to the 2 circumferences in close proximity. On the contrary, through the length of the cylinders, a significant standard deviation was obtained since the ends of the filament wound structure appear to be less compacted, as also observed in Fig.8.

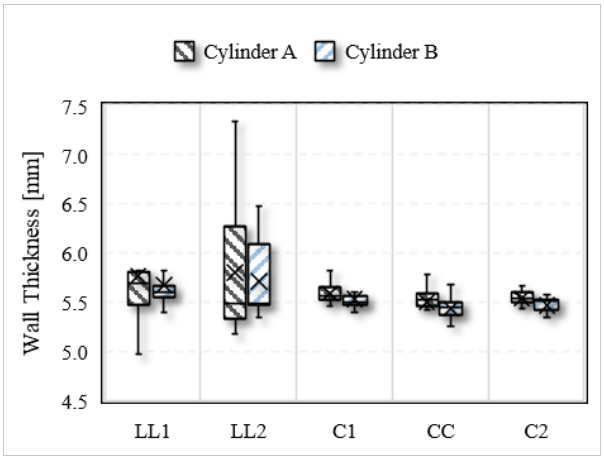

Fig. 10: The average values of the thickness obtained by the ultrasound inspection of the 5 point lines of the 2 cylinders.

4.2.2 Discontinuities inside the structure

As stated in the previous section, due to the complex nature of a filament wound cylinder some discontinuities are identified inside the structure. These appear as multiple peaks in the A-Scan between the initial pulse and the backwall echo. ~~In some cases, the discontinuities have an extent that do not permit the identification of the backwall echo.~~

The distribution of the discontinuities across the longitudinal directions is presented in Fig. 11. The graphs show that the discontinuities are present at almost all the measuring points. In Cylinder A the discontinuities are 20 along LL1 direction and the same number is identified along the LL2 direction. These are located between 1.5 mm to 4 mm inside the structure. In Cylinder B at 27 defects points along both directions are identified echoes indicating the presence of a gap. These are located between 1and 4 mm from the external surface. Along direction LL2 of cylinder B the discontinuities tend to increase their depth inside the structure from point 11 to 16 and then decrease until point 22. As shown in Fig.11, in some cases discontinuities tend to cluster at the same depth in three measuring points. For example, from point 4 to 6 in LL1 direction of Cylinder A. The same behavior is present in points 10 to 12 of LL1 direction of Cylinder 2.

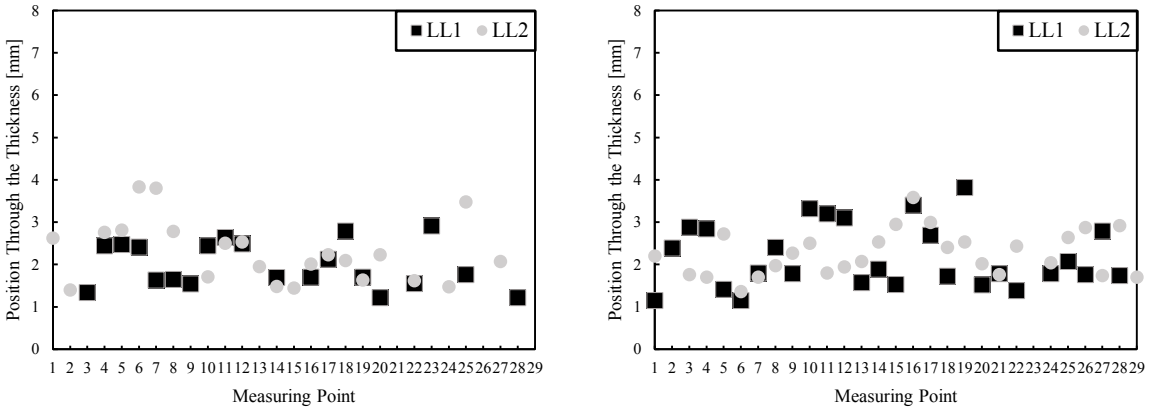

Fig. 111: Distribution of the discontinuities inside the structure of the wound cylinders along the longitudinal directions: (a) Cylinder A; (b) Cylinder B

The discontinuities along the circumferential directions CC, C1 and C2 of the cylinders are presented in Fig. 12 for the Cylinder A (Fig.12(a)) and for Cylinder B (Fig.12(b)). Regarding the Cylinder A, the discontinuities are distributed between 0.6 mm to 3.2 mm. From the graph, there are more defects along the CC direction since these are present in all the measuring points. Cylinder B has more discontinuities, and this is highlighted by the figure. In this case, the defects are in a depth that ranges from 1.5 mm to 3.7 mm. In Cylinder B all the considered directions have discontinuities in all the measured points.

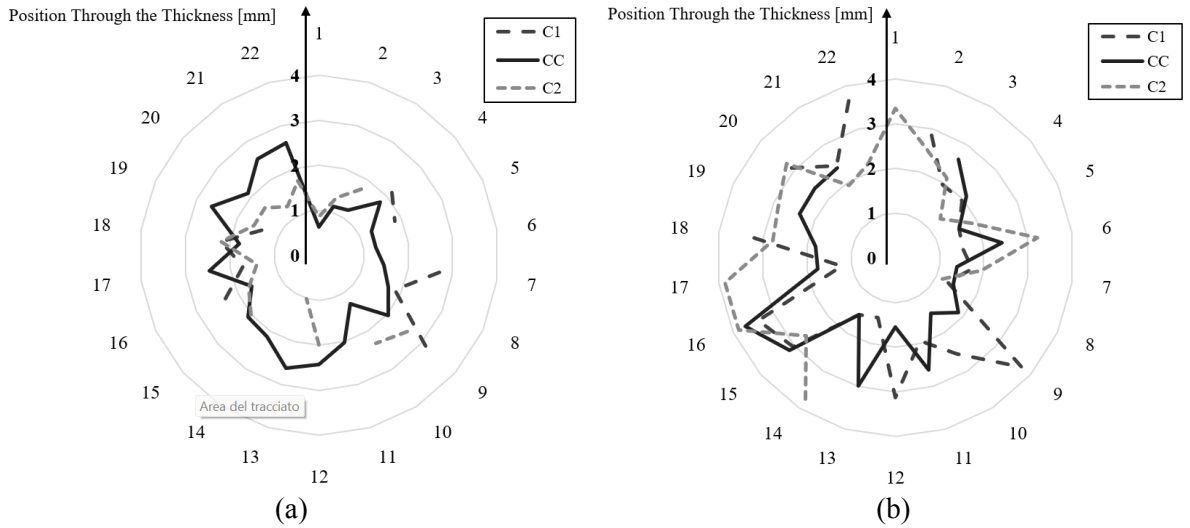

Fig. 122: Distribution of the discontinuities inside the structure along the circumferential directions: (a) Cylinder A; (b) Cylinder B

The presence of defects inside the structure of both cylinders may be considered as a process-driven effect. In fact, during the winding process, gaps between adjacent tows of the same layer may be created as well as folding of the deposited tows while the machine deposition head changes direction at the ends

of each cylinder. The combination of these 2 phenomena may also explain the position through the length and thickness of the defects observed, especially in the case of the Cylinder B, also considering the compaction at the zones close to the 2 ends of the cylinders is relatively lower compared to the central part.

4.2.3 Winding Angle

A typical winding angle distribution through the length of the filament wound cylinders is presented in Fig. 11. The local measurements are accompanied by the standard deviation as obtained by the optical inspection utilizing the vision-based system. Even in the case of the winding angle, the hollow cylinder may be divided into 3 sections, one at the central part (between the 6th and the 17th points) and the 2 ends where the winding angle achieved values way higher than the nominal one. In fact, the winding angle is gradually increasing as moving from the central part of the cylinder towards the external zones.

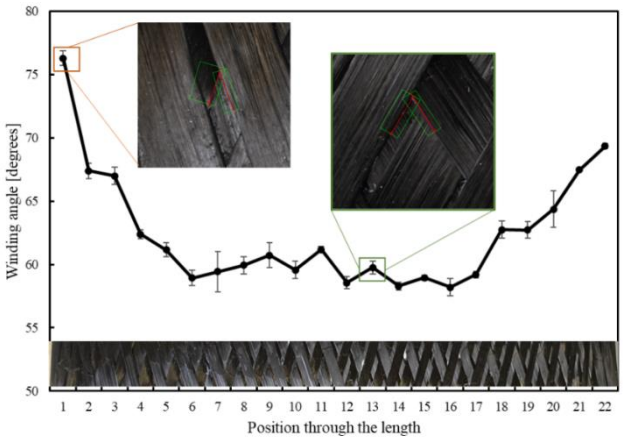

Fig. 13: Typical distribution of the winding angle through the length of the filament wound cylinder and detailed view of the 76^o and 60^o of the local points.

An interesting aspect of the winding angle concerns its variation through the length of the hollow cylinders in different zones as well as through the central circumferences. As seen in Fig.12, the winding angle follows similar trends through the length of both cylinders regardless of the location of the point lines. On the contrary, the optically measured winding angle is almost invariant in the 3 circumferences.

Cylinder A	Cylinder B

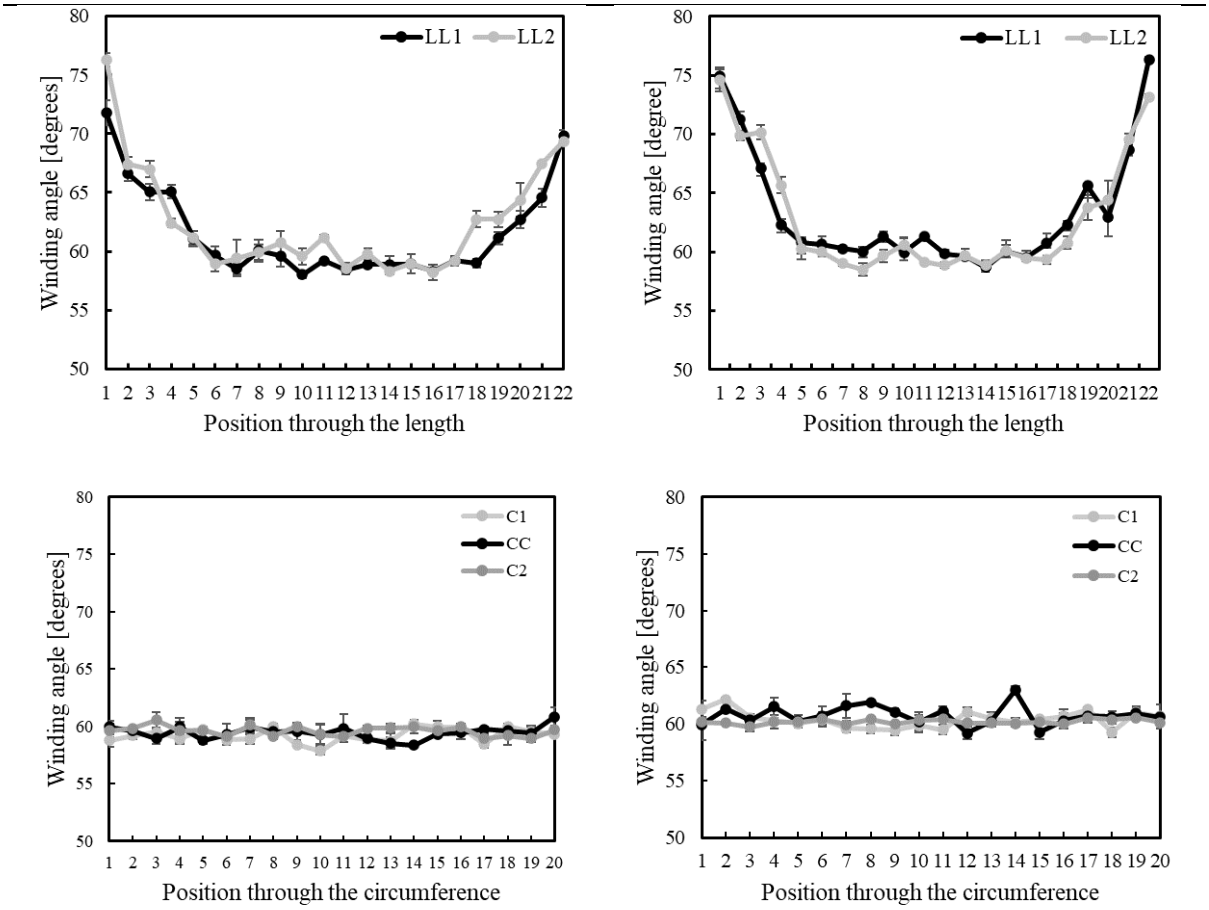

Fig. 14: Distribution of the winding angle through the length and through the circumferences of the 2 composite cylinders,

Similar observations may be extracted from the average values of the box plot of Fig. 13 where the average winding angle and the corresponding standard deviations are reported. The 3 circumferences are demonstrating average values close to the nominal one (60^o) with a low standard deviation. On the contrary, the tows' winding angle appears to be variable through the length achieving average values of 62^o and 64^o for the Cylinder A and B respectively, accompanied also by an extensive standard deviation. Therefore, the actual filament winding angle may be considered variable only through the length of the hollow composite cylinders and not through the circumference of a certain point through the length of them.

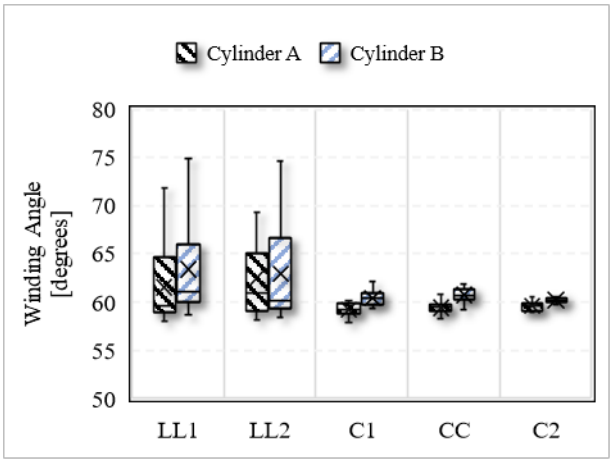

Fig. 15: The average values of the tows winding angle as measured by the vision-based system through the length (LL1, LL2) and the circumferences of the 2 cylinders.

5. Conclusions

In the present work, a study of the morphological characteristics of as-manufactured helicoidally filament wound cylinders made of carbon fiber and epoxy towpregs was presented using contact and non-contact measurements techniques. The contact-based ultrasound inspection was utilized for measuring the actual of the components and to verify the presence of discontinuities inside the composite structure. A non-contact vision-based measuring technique was implemented to assess the winding angle of the components.

The main results of this morphological analysis are the presence of a thickness variation along the longitudinal directions of the cylinder. In the ending parts the components are thicker, far from the nominal values. Therefore, the external parts through-the-length of the hollow composite cylinder appear to be less compacted compared to the central part. In fact, the variation between the circumferences situated near the central part was found to be much less. Consequently, the compaction of the deposited filaments, presumably due to the characteristics of the filament winding machine and its relative movable parts, is found to be variable. Moreover, several discontinuities are detected through the thickness, exclusively in the zones of the helicoidally wound part (mostly from 1 to 4 mm from internal to external surface). This phenomenon is attributed to the discontinuity created between consecutive tows that create an interlaced structure with a gap between them.

In addition, the winding angle was measured through the length and circumference of the 2 as-manufactured cylinders. The results revealed a significant variation between the 2 ends of the cylinders and the internal part, having a difference of roughly 15^{o}. Even in this case, the difference between the central part and the 2 ends may be explained by the relative movement of the deposition head of the machine and the rotational speed of the mandrel.

To conclude with, also considering the uncertainty assessment of the measuring techniques that indicates that the obtained data is reliable, both the 2 techniques are valid and may be further exploited for characterizing the filament wound products and for ameliorating the process characteristics. The obtained information is useful for the process characterization and can be used to improve it.

Acknowledgments

This work was funded by the National Italian project "*Smart Tow Winding – Nuove soluzioni ad elevata automazione per l'impregnazione e l'avvolgimento di tow*" – European Union, Fondo Europeo di Sviluppo Regionale, Project Code: ARS01_00871.

References

1. Zhang N., Zhao Q., Mi Z., Wang Y., Gu B. "Axial impact compressive behaviors of a novel 3-D integrated multilayer fabric reinforced composite tubular structures." Thin-Walled Structures 134: 363–372 (2019). DOI: 10.1016/j.tws.2018.10.037
2. Azeem M., Ya H.H., Alam M.A., Kumar M., Stabla P., Smolnicki M., Gemi L., Khan R., Ahmed T., Ma Q., Sadiqu Md R., Mokhtar A.A., Mustapha M. "Applications of filament winding technology in composite pressure vessels and challenges: A review." Journal of Energy Storage 49, 103468 (2022). Doi: 10.1016/j.est.2021.103468
3. Pandita S.D., Irfan M.S., Machavaram V.R., Shotton-Gale N., Mahedran R.S., Wait C.F., Paget M.A., Harris D., Leek C., Fernando G.F. "Clean filament winding-Part I: Design concept and simulations." Journal of Composite Materials 47 (3), 379-390. Doi: 10.1177/0021998312440474
4. Funck R. and Neitzel M. "Improved thermoplastic tape winding using laser or direct-flame heating." Journal of Energy Storage 49, 103468 (2022). Doi: 10.1016/j.est.2021.103468
5. Khennane A. "Filament winding processes in the manufacture of advanced fibre reinforced polymer composites." Advanced fibre-reinforced polymer composites for structural applications. Woodhead publishing series in civil and structural engineering, Chapter 8, Woodhead Publishing, 187–206 (2013). Doi: 10.1533/9780857098641.2.187
6. Duval M., Ramani K., Bays M., Caillat F. "In-situ composite manufacture using an electrostatic powder spray process and filament winding." Polymers and Polymer Composites 4 (5), 325-334 (1996). Doi: 10.1177/096739119600400505
7. DuVall F.W. "Cost comparison of wet filament winding versus prepreg filament winding for type II and type IV CNG cylinders." Sampe Journal 37(1), 38-42 (2001).
8. Scott A.E., Sinclair I., Spearing S.M., Mavrogordato M.N., Hepples W. "Influence of voids on damage mechanisms in carbon/epoxy composites determined via high resolution computed tomography." Composites Science and Technology 90, 147-153 (2014). Doi: 10.1016/j.compscitech.2013.11.004
9. Faria H. "Analytical and numerical modelling of the filament winding process." PhD Thesis, Universidade do Porto, Faculdade de Engenharia (2013)
10. Stecenko T.B., Piggot M.R. "Fiber misalignment in filament wound tubes." Materials Science Forum 282-283, 257-262 (1998). Doi: 10.4028/www.scientific.net/msf.282-283.257
11. Stecenko T.B., Piggot M.R. "Fiber waviness and other mesostructures in filament wound materials." Journal of Reinforced Plastics and Composites 16 (18), 1659-1674 (1997). Doi: 10.1177/073168449701601803
12. Wang Y., Feng J., Wu J., Fu D. "Effects of fiber orientation and wall thickness on energy absorption characteristics of carbon-reinforced composite tubes under different loading conditions." Composite Structures 153, 356-368 (2016). Doi: 10.1016/j.compstruct.2016.06.033
13. Johnson E.C. and Nokes J.P. "Nondestructive evaluation (NDE) techniques assessment for graphite/epoxy (Gr/Ep) composite overwrapped pressure vessels." Report no. A162362, Space and Missile Systems Center, Air Force Materiel Command, (1998).
14. Downs K.S. and Hamstad M.A. "Acoustic emission from depressurization to detect/evaluate significance of impact damage to graphite/epoxy pressure vessels." Journal of Composite Materials 32 (3), 258-307 (1998). Doi: 10.1177/002199839803200304
15. Lee Y.J., Ahmed H., Lee J.R. "Acoustic emission from depressurization to detect/evaluate significance of impact damage to graphite/epoxy pressure vessels." Composite Structures 236, 111871 (2020). Doi: 10.1016/j.compstruct.2020.111871
16. Srivastava C., Agostino P., Stamopoulos A.G., Alcock B., Strandlie A., Grammatikos S. "Three-dimensional analysis of porosity in as-manufactured glass fiber/vinyl ester filament winded composites using X-Ray micro-computed tomography". Applied Composite Materials (2023). Doi: 10.1007/s10443-023-10167-z.
17. Tosti E. "UT in phased array applications for control of structures and piping of stages in the European Space Launchers." 12th European Conference on Non-Destructive Testing (ECNDT 2018), Gothenburg 2018, June 11-15. e-Journal of Nondestructive Testing Vol. 23(8). https://www.ndt.net/?id=22998:
18. Mihaljević M., Markučič D., Runje B.,Keran, Z. "Measurement uncertainty evaluation of ultrasonic wall thickness measurement. " Measurement 137, 179-188 (2019). Doi: 10.1016/j.measurement.2019.01.027

19. Samaitis V., Yilmaz B., Jasiuniene E. “Adhesive bond quality classification using machine learning algorithms based on ultrasonic pulse-echo immersion data.” Journal of Sound and Vibration 546, 117457 (2023). Doi: 10.1016/j.jsv.2022.117457
20. Stamopoulos A., Chiominto L., Natale E., Di Ilio A., D’Emilia G. “Identification of the characteristics of helicoidally filament wound tubes using vision systems.” Procedia Computer Science, 217, 1048-1056 (2023). Doi: https://doi.org/10.1016/j.procs.2022.12.303
21. Yao X.F., Meng L.B., Jin J.C., Yeh H.Y. “Full-field deformation measurement of fiber composite pressure vessel using digital speckle correlation method.” Polymer Testing 24 (2), 245-251 (2005). Doi: 10.1016/j.polymertesting.2004.05.009
22. Wróbel B and Pawlak S. “A comparison study of the pulse-echo and through-transmission ultrasonics in glass/epoxy composites.” Journal of Achievements in Materials and Manufacturing Engineering 22 (2), 51-54 (2007).
23. Benstock D., Cegla F., Stone M. “The influence of surface roughness on ultrasonic thickness measurements.” The Journal of the Acoustical Society of America, 136(6), 3028-3039. (2014). Doi: 10.1121/1.4900565
24. D’Emilia G., Gaspari A., Natale E., Stamopoulos A.G., Di Ilio A. “Experimental and numerical analysis of the defects induced by the thermoforming process on woven textile thermoplastic composites.” Engineering Failure Analysis 135, 106093 (2007). Doi: 10.1016/j.engfailanal.2022.106093
25. Mertiny P. and Ellyin F. “Influence of the filament winding tension on physical and mechanical properties of reinforced composites.” Composites Part A: Applied Science and Manufacturing 33 (12), 1615-1622 (2002). Doi: 10.1016/S1359-835X(02)00209-9
26. Blachut A., Wollmann T., Panek M., Vater M., Kaleta J., Detyna J., Hoschutzky S., Gude M. “Influence of fiber tension during filament winding on the mechanical properties of composite pressure vessels.” Composites Structures 304 (1), 1163372 (2023). Doi: 10.1016/j.compstruct.2022.116337